THE JOURNAL OF PHYSICAL CHEMISTRY LETTERS
A JOURNAL OF THE AMERICAN CHEMICAL SOCIETY

pubs.acs.org/JPCL Letter

Synthesis and Properties of Stable Amino Metal Halide Molecular Clusters in the Solid State

Heng Zhang, Evan Thomas Vickers, Samuel Erickson, Melissa Guarino-Hotz, Jeremy Lake Barnett, Sayantani Ghosh, and Jin Zhong Zhang*

Cite This: J. Phys. Chem. Lett. 2022, 13, 10543−10549 Read Online

ACCESS | Metrics & More | Article Recommendations | Supporting Information

ABSTRACT: Nanosized molecular clusters (MCs) composed of $PbBr_2$ and neutral ligand butylamine (BTYA) with unique optical properties in solution and solid states have been synthesized using ligand-assisted reprecipitation and spin-coating, separately. The studies of their optical properties using ultraviolet−visible (UV−vis) absorption and photoluminescence (PL) show the first electronic absorption and PL band of the MCs at 401 and 411 nm, respectively, for the solution and solid state samples that exhibit good stability under ambient conditions. Low-temperature PL spectra below 30 K show vibronic peaks indicative of a single size or a very narrow size distribution of the MCs. On the basis of Raman, X-ray diffraction, and transmission electron microscopy measurements, a layered structural model is proposed for the MCs with a BTYA ligand capping on the surface of the corner-shared tilted $[PbBr_6]^{4-}$ octahedral framework. The stable and retained structure of MCs in the solid state is promising for photonics applications.

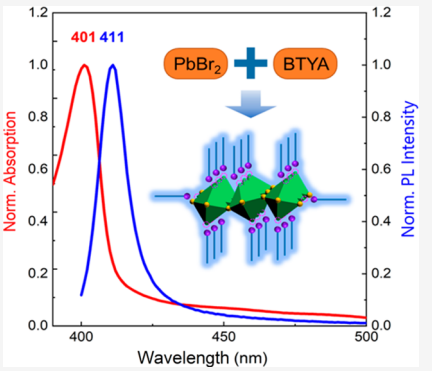

Molecular clusters (MCs) are small particles with a single size or a very narrow size distribution.[1−3] They have attracted considerable interest due to their unique properties, including their tunable size and shape at the molecular scale and the possibility of serving as building blocks for larger structures such as nanocrystals (NCs) or bulk crystals. Recently, MCs based on metal halides and capping ligands have been reported. For example, Zhou et al. synthesized $(C_9NH_{20})_7(PbCl_4)Pb_3Cl_{11}$ metal halide clusters exhibiting blue emission that peaked at 470 nm with cationic ligand $C_9NH_{20}^+$, showing a photoluminescence quantum efficiency (PLQE) of 83 ± 1%.[1] Vickers et al. found PbX_2-BTYA (X = Cl^-, Br^-, or I^-) MCs with a PbX_2 framework capped with neutral ligand butylamine (BTYA), which lack the A component in the conventional metal halide perovskite (MHP) ABX_3 (A = Cs^+ or MA^+, B = Pb^{2+} or Sn^{2+}, and X = Cl^-, Br^-, or I^-) formula.[2] They exhibit bluer absorption and emission bands compared with those of MHP NCs,[4,5] quantum dots (QDs),[6−8] or magic sized clusters (MSCs)[9−11] due to their smaller size, over the ranges of 335−515 nm for absorption peaks and 344−519 nm for photoluminescence (PL) peaks depending on the halides. Their ultrasmall size and sharp absorption and emission bands, with a full width at half-maximum (fwhm) around 10 nm, are attractive for potential photonics applications such as blue single-photon emitters.[2,3,12]

Earlier attempts have been made to determine the structure of the PbX_2-BTYA MCs using the extended X-ray absorption fine structure (EXAFS) technique, and several tentative structural models were proposed.[2] However, it has been challenging to determine their structure directly using techniques such as X-ray diffraction (XRD) and transmission electron microscopy (TEM) because the MCs tend to grow into larger structures or aggregate upon drying into a solid form.[2,3,13,14] Producing isolated MCs in the solid state is essential for their structural determination as well as for device applications.

In this work, we report the first successful synthesis and characterization of isolated MCs based on $PbBr_2$ and neutral capping ligands BTYA in the solid state that have optical properties identical to those of MCs in the solution state. Structural studies based on Raman, XRD, and TEM led to the proposal of a structural model based on a layered structure with corner-shared tilted $[PbBr_6]^{4-}$ octahedra and BTYA capping ligands on the surface. Vibronic features in low-temperature PL data provide evidence of exciton−phonon coupling and a single size or a very narrow size distribution of the MCs. Good stability is observed under ambient conditions, which is attributed to the strong ligand coordination effect on the $[PbBr_6]^{4-}$ octahedral surface.

Figure 1 shows the absorption and PL spectra of $PbBr_2$-BTYA MCs in solution and solid states. For MCs in solution, as shown in Figure 1a, the first absorption and PL emission

Received: September 28, 2022
Accepted: November 1, 2022
Published: November 7, 2022

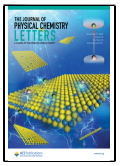

https://doi.org/10.1021/acs.jpclett.2c02977
J. Phys. Chem. Lett. 2022, 13, 10543−10549

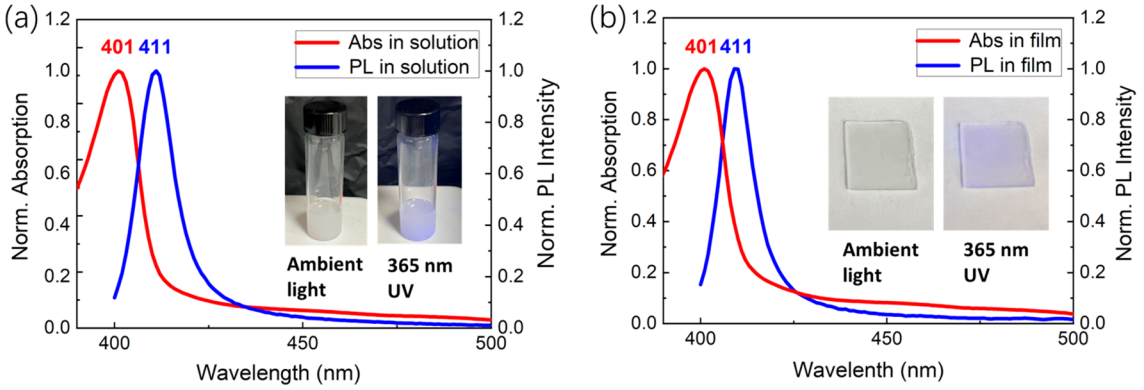

Figure 1. Optical properties of $PbBr_2$-BTYA MCs in solution and solid states. (a) UV−vis absorption spectra and PL spectra of $PbBr_2$-BTYA MCs in the solution state. The insets are images of MCs in the solution state under ambient light and 365 nm UV light. (b) UV−vis absorption spectra and PL spectra of $PbBr_2$-BTYA MCs in the solid state. The insets are images of MCs in the solid state under ambient light and 365 nm UV light.

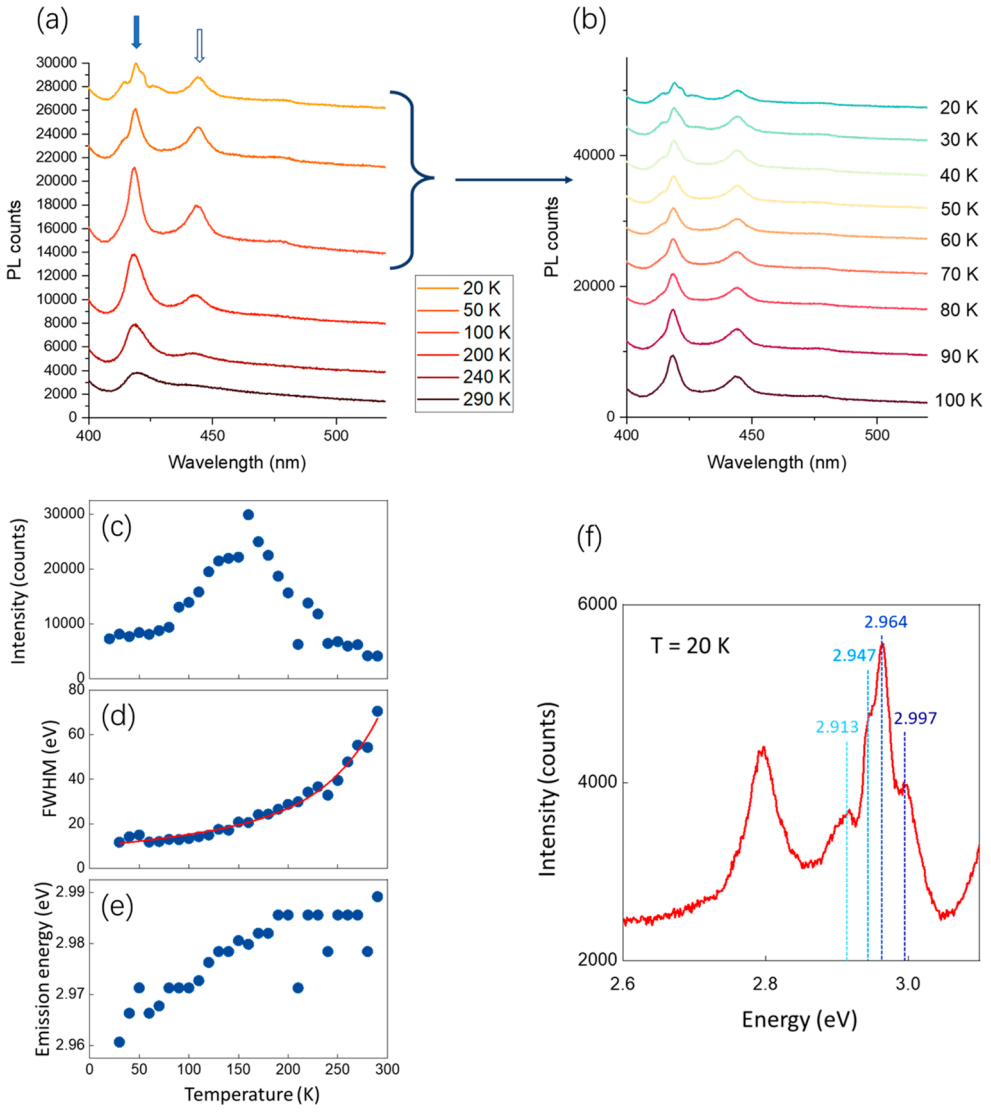

Figure 2. Low-temperature-dependent PL spectra of the film of $PbBr_2$-BTYA MCs. (a) PL spectra that are dependent on temperature from 20 to 290 K and two main peaks around 416 and 440 nm that red-shift gradually as the temperature decreases. (b) PL spectra focused on temperatures from 20 to 100 K, among which the interval is 10 K. (c) PL intensity, (d) fwhm, and (e) emission energy based on different temperatures from 20 to 290 K. (f) PL spectra focused on the 444 nm (left main peak) and 418 nm (right main peak) bands with several shoulder peaks around the 418 nm band at 20 K.

https://doi.org/10.1021/acs.jpclett.2c02977
J. Phys. Chem. Lett. 2022, 13, 10543−10549

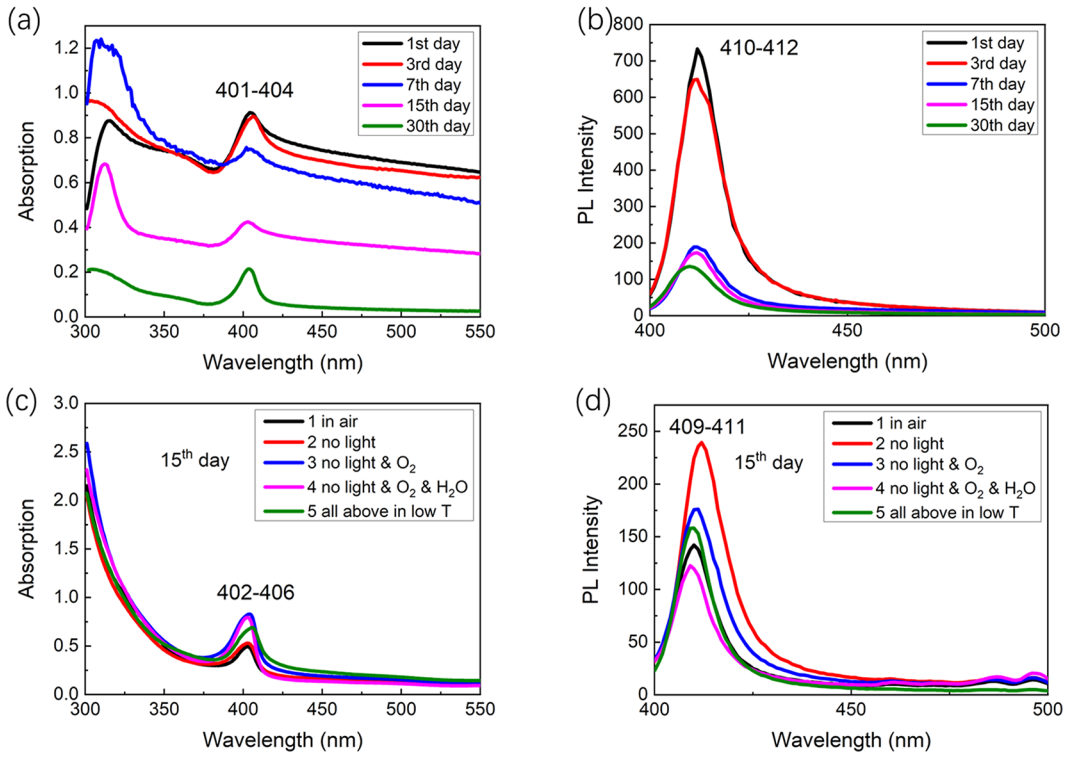

Figure 3. Stability of $PbBr_2$-BTYA MCs in solution and solid states. (a) UV−vis absorption spectra and (b) PL spectra of $PbBr_2$-BTYA MCs in the solution state. (c) UV−vis absorption spectra and (d) PL spectra of $PbBr_2$-BTYA MCs in the solid state stored for 15 days under five different ambient conditions: in air (1), without light (2), without light and oxygen (3), without light, oxygen, and moisture (4), and without light, oxygen, and moisture at a low temperature (0 °C) (5).

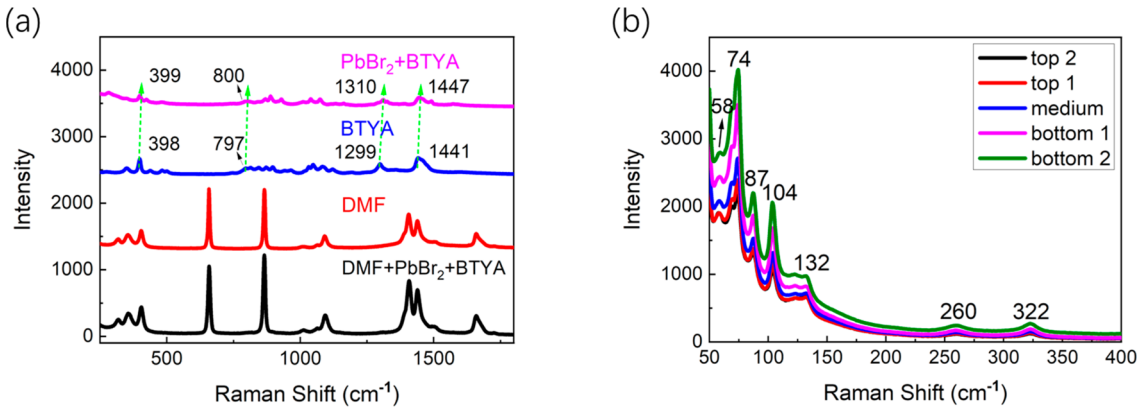

Figure 4. Raman spectra of $PbBr_2$-BTYA MCs at high and low vibrational frequencies to show ligand interactions and MC phonon vibrational frequencies, respectively. (a) Raman spectra of components of $PbBr_2$-BTYA MCs in the solution state (solvent DMF, ligand BTYA, mixture of $PbBr_2$ powder and the BTYA solution, and $PbBr_2$-BTYA MCs in solution). (b) Raman spectra of $PbBr_2$-BTYA MCs in the solid state at different *Z* axis heights.

Table 1. Assignments for Raman Peaks of Solid $PbBr_2$-BTYA MCs

Raman shift (cm^{-1})	assignment
58	octahedral distortion
74	butylamine lurching
87	butylamine lurching
104	butylamine lurching
132	butylamine lurching
260	C−N torsion
322	C−N torsion

peaks are at 401 and 411 nm, respectively, and the PL band has an fwhm of 10 nm, which is in good agreement with previous reports by our group and indicates a single or narrow size distribution of MCs.[2,3] The PL Stokes shift is only 10 nm, indicating a low density of defects within the bandgap due to strong passivation of the surface with the BTYA ligand.[3,15] More interestingly, when we transfer the sample from the solution to solid state using spin-coating, the absorption and the emission peaks do not shift at all, as shown in Figure 1b. This is significant because it indicates that the MCs in the solid state retain their properties as in solution, which is crucial for device applications because the solid state is the form that is usually required. As reported previously, clusters tend to grow

https://doi.org/10.1021/acs.jpclett.2c02977
J. Phys. Chem. Lett. 2022, 13, 10543−10549

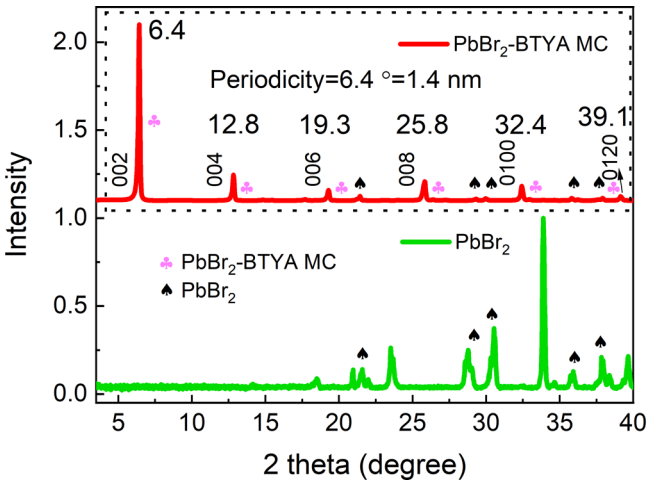

Figure 5. X-ray diffraction pattern of the $PbBr_2$-BTYA MC film and $PbBr_2$ film. The club sign stands for the $PbBr_2$-BTYA MC phase, and the spade sign stands for the $PbBr_2$ phase.

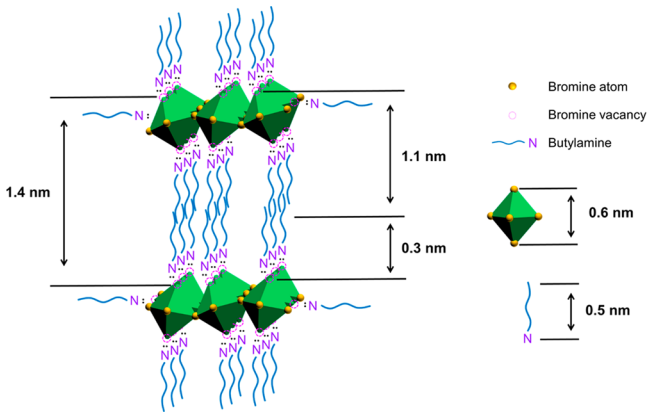

Figure 7. Proposed layered structure for $PbBr_2$-BTYA MCs capped with the BTYA ligand. The Br atoms on the surface are replaced by N atoms in BTYA mostly on the top and bottom sides of the $[PbBr_6]^{4-}$ octahedral framework through a N−Pb coordination bond. Some lateral sides of the Br atom can also be replaced by N atoms due to the electroneutrality principle.

into a larger structure or aggregate upon drying into a solid form from solution.[2,3,13,14,16,17]

To confirm that the formation of MCs involves both $PbBr_2$ and BTYA, a series of control experiments were conducted. First, the UV−vis absorption and PL spectra of a solution of toluene, DMF, BTYA, and MC precursors were characterized. As shown in panels a and b of Figure S1, there are no peaks observed in the absorption or PL spectra for a pure solution of toluene, DMF, or BTYA in the spectral range of 300−800 nm. For the MC precursor solution, broad absorption and emission bands are observed, indicating the interaction between $PbBr_2$ and BTYA in solution in the form of different kinds of lead bromide complexes assisted by BTYA, for example, $PbBr_3^-$ and $PbBr_4^{2-}$.[18] However, there are no sharp spectral features observed, indicative of the formation of nanocrystals or nanoclusters with regularly arranged microscopic structures.[17] Moreover, panels c and d of Figure S1 show a comparison of the UV−vis and PL spectra of $PbBr_2$ and $PbBr_2$-BTYA MCs in solution and solid states. Only the solution of $PbBr_2$-BTYA MCs and the film sample exhibit characteristic peaks, which clearly indicates that the spectral features of MCs around 400 nm originate from a combination of $PbBr_2$ and BTYA, not $PbBr_2$ alone.

Figure 2 shows low-temperature-dependent PL spectra from 20 to 290 K. In Figure 2a, at 290 K, a single emission peak is observed at 416 nm (indicated by a solid blue arrow), which we identify as arising from band edge recombination. The slight red-shift of the 416 nm peak compared with the 411 nm peak is possibly due to the use of different PL instruments that may not be calibrated identically. When $T < 240$ K, a second low-energy (longer wavelength) peak can be seen centered at 440 nm (hollow blue arrow), which persists down to 20 K. This could be attributed to shallow surface defect-related trap states[9,19] or self-trapped exciton (STE) states,[20,21] which are ~160 meV below the conduction band according to the difference in energy between the 416 nm peak and the red-shifted 440 nm peak. Figure 2b focuses on PL in the range of 20−100 K to highlight the change in the band edge emission intensity as the temperature is decreased.

Panels c−e of Figure 2 show the spectral analysis of the PL data at low temperature. The emission intensity, spectral fwhm, and peak emission energy are plotted with temperature in panels c−e of Figure 2, respectively. The minor blue-shift of the emission energy with an increase in T could be due to thermally induced excitonic emission.[22] The spectral broadening indicated by the fwhm increasing with T is expected with increased inhomogeneous broadening. However, while the

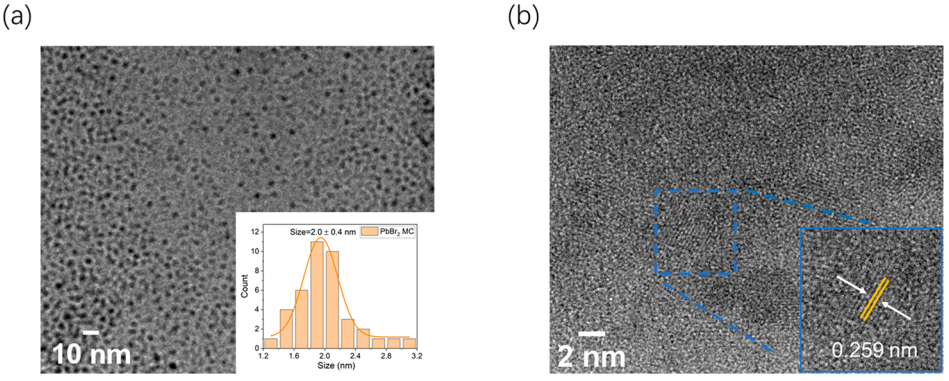

Figure 6. TEM images of $PbBr_2$-BTYA MCs. (a) TEM images of $PbBr_2$-BTYA MC films. The inset shows the size distribution of MCs. (b) High-resolution TEM (HRTEM) images of $PbBr_2$-BTYA MC films showing the crystal lattice. The inset shows an enlarged HRTEM image showing the interplanar spacing along the (010) planes.

https://doi.org/10.1021/acs.jpclett.2c02977
J. Phys. Chem. Lett. 2022, 13, 10543−10549

peak energy and fwhm monotonically change with T, the emission intensity shows a clear maximum around 160 K.

The fwhm is fitted to[22]

$$\Gamma(T) = \Gamma_O + \sigma T + \frac{\Gamma_{op}}{e^{E_p/k_B T} - 1}$$

where $\Gamma(T)$ is the fwhm, Γ_O is the inhomogeneous contribution, σ and Γ_{op} are the excitonic coupling constants for acoustic and optical phonons, respectively, and E_p is the optical phonon energy. The fitting reveals σ to be insignificant, implying that the optical phonon contributions dominate. The phonon energy is approximately 64 meV.

Figure 2f zooms in on the band edge PL at 20 K and reveals a series of closely spaced emission peaks. From the lowest-energy peak at 2.913 eV, the spacings are roughly 34 meV (274 cm^{-1}), 17 meV (137 cm^{-1}), and 33 meV (266 cm^{-1}), all close to phonon frequencies to be discussed below. These vibronic peaks indicate strong exciton−phonon coupling and that the MCs are a single size or have a very narrow size distribution, because such features would not be expected if there were a broad size distribution.

The stability of the MCs was studied by monitoring their absorption and PL spectra over time under different conditions involving light, oxygen, and moisture factors.[23−25] First, the stability of $PbBr_2$-BTYA MCs in their native environment was studied, in which MCs are precipitates in the solution state. All of the samples were kept in an ambient environment (room temperature and 1 atm) and characterized without further protection. Panels a and b of Figure 3 show the UV−vis and PL spectra, respectively, of $PbBr_2$-BTYA MCs in the solution state within 30 days. There is a small variation in the peak position in both absorption and PL spectra, which is attributed to subtle size changes during storage.[2,15] The intensity of both absorption and PL decreases over time. On the 30th day, the intensity is only at 20% of its initial intensity, suggesting the degradation of the emissive MCs in solution in the ambient environment. Interestingly, the MCs did not seem to grow or aggregate in solution because the spectral position does not change over time, with the peaks shifting only 2−3 nm within 30 days, reflecting the structural stability of isolated MCs due to strong ligand passivation.[2,3,17]

To study the stability of MCs in the solid state, a series of experiments under different conditions were conducted for ≤45 days, including film samples stored in air (1), without light (2), without light and oxygen (3), without light, oxygen, and moisture (4), and without light, oxygen, and moisture at a low temperature (0 °C) (5). Panels c and d of Figure 3 show the absorption and PL spectra, respectively, of all of the $PbBr_2$-BTYA MCs on the 15th day (detailed stability test results within 45 days are shown in Figures S2 and S3). The absorption and emission peaks fluctuate within a narrow range (absorption peaks at 4 nm, while PL peaks at 2 nm) for all five samples, which was attributed to subtle size differences upon synthesis. Surprisingly, the individual sample does not experience any peak change over 15 days, which indicates the MCs are stable and the original structure is retained even in the ambient environment. This stability is attributed to the strong coordination of the N atom in the BTYA ligand to Pb^{2+}, which also provides exceptional passivation for the metal halide surface defects.[26] According to the absorption and PL spectra in Figures S2 and S3, respectively, the intensity decreases gradually as the storage time increases. The solid control samples in air show no optical properties for absorption or emission on the 30th day due to the degradation. However, when light irradiation alone is excluded, it is possible to elongate the emissive properties to 45 days. Therefore, light plays a key role in the long-term stability of $PbBr_2$-BTYA MCs. Other variables such as oxygen, moisture, and low temperature deteriorate the stability less compared with light during the 45 day test.

Raman spectroscopy and XRD were utilized to provide structural information about the MCs. First, $PbBr_2$-BTYA MCs were characterized in solution in the high-Raman vibrational frequency region to understand the interaction between the ligand and $PbBr_2$. Figure 4a shows the Raman spectra of the solvent DMF, ligand BTYA, the mixture of $PbBr_2$ powder and the BTYA solution, and the solution of $PbBr_2$-BTYA MCs ($PbBr_2$ powder and the BTYA solution were dissolved in the DMF solvent first and then precipitated in toluene). Comparing DMF and $PbBr_2$-BTYA MC solution, we find the spectra are dominated by peaks from DMF, which is likely due to the dominance of DMF in the solution. Comparing the BTYA solution with the $PbBr_2$/BTYA solution, we find the peaks of the BTYA solution at 398, 797, 1299, and 1441 cm^{-1} shift to higher vibrational frequencies in the $PbBr_2$/BTYA solution. These peaks are ascribed to C−N torsion, NH_2 torsion, C−H_2 twist, and C−H_2 bending, respectively.[27,28] This shift in the $PbBr_2$/BTYA solution suggests the interaction between the BTYA ligand and $PbBr_2$, likely through the amine group.[29]

The $PbBr_2$-BTYA MCs were characterized in the solid state in the low-Raman vibrational frequency region to determine the vibrational phonon modes of MCs. Figure 4b shows several vibrational peaks at low frequencies on different thicknesses of solid films. The peak assignments are summarized in Table 1. The peaks retain the same position on different film thicknesses, indicating the same structure of MCs on different thicknesses of films and confirming the interaction between the ligand and octahedra. On the basis of the assignments, an initial structure is proposed with corner-shared tilted $[PbBr_6]^{4-}$ octahedra as the framework and the BTYA ligand interacting with Pb^{2+} on the surface.

XRD was used to determine the crystal structure of $PbBr_2$-BTYA MCs. The diffraction pattern of $PbBr_2$-BTYA MCs exhibits peaks at 6.4°, 12.8°, 19.3°, 21.4°, 25.8°, 32.4°, 35.8°, and 39.1° (Figure 5), which is different from conventional diffraction peaks of perovskite $CsPbBr_3$ crystals or $MAPbBr_3$ crystals at 15.3°, 21.7°, and 30.7°.[30,31] This demonstrates that MCs formed a crystalline structure that is different from the cubic structure of a conventional ABX_3 perovskite.[30] In addition, the contrast with the pure $PbBr_2$ crystal illustrates that $PbBr_2$-BTYA MCs no longer retain the $PbBr_2$ orthorhombic structure, which confirms interaction between the ligand BTYA and $PbBr_2$ (the pure $PbBr_2$ XRD data were compared to the JCPDS PDF 31-0679). Interestingly, the XRD peaks show regular degree intervals of 6.4°, which corresponds to a 1.4 nm distance according to Bragg's law. This XRD result matches the reported layered Ruddlesden−Popper $(BA)_2PbBr_4$ (BA = butylammonium) perovskite crystals when the number of metal halide octahedral layers is one.[32−34] It is also similar to other reported layered structures that show the close XRD peak positions and regular XRD peak degree interval.[35] All of the reports show not only comparable XRD results but also analogous optical absorption and emission properties. This led us to propose that the $PbBr_2$-

https://doi.org/10.1021/acs.jpclett.2c02977
J. Phys. Chem. Lett. 2022, 13, 10543−10549

BTYA MCs have a similar layered structure as depicted in Figure 7.[32−36]

Figure 6 shows TEM images of $PbBr_2$-BTYA MCs. On the basis of images of 40 MCs in Figure 6a, an average size of 2.0 ± 0.4 nm is calculated. Figure 6b shows the high-resolution TEM (HRTEM) image of the MCs that reveal clear lattice fringes indicating the good crystallinity of the $PbBr_2$-BTYA MCs. The interplanar spacing is measured to be 0.259 nm, which corresponds to the (010) crystal plane and proves that octahedra are tilted between two adjacent (010) planes because one Pb−Br bond is ∼0.3 nm in length in the Br shared Pb−Br−Pb bond between two octahedra.[33] The TEM results confirm the crystal size and crystalline nature of $PbBr_2$-BTYA MCs, rather than disordered or amorphous as one might expect on the basis of their expected molecular nature.

On the basis of the structural characterizations presented above, we propose a structure for the MCs based on corner-shared tilted octahedra as the framework and the BTYA ligand for coordination and passivation on the surface, as illustrated in Figure 7. The $[PbBr_6]^{4-}$ octahedra are tilted on the basis of Raman vibrational frequencies and interplanar spacing from HRTEM. The lone pair electrons in the N atom in the amine group of the BTYA ligand likely coordinate with Pb^{2+} to form a stable complex.[26] BTYA also serves as a capping ligand for cationic defects on the surface like a Br^- vacancy. van der Waals interaction between hydrocarbon tails of BTYA likely leads to the formation of stable layered structures.[34,37]

In summary, stable nanosized $PbBr_2$-BTYA MCs have been synthesized in the solid and solution states and show identical absorption and emission properties. The results indicate that the MCs have the same structure in the solid and solution states, unlike other small clusters synthesized in solution, which often tend to grow into a larger structure or aggregate upon drying to a solid, making them challenging for applications. MCs have narrow electronic absorption and emission bands with a small Stokes shift, suggesting the low density of defects due to strong surface passivation. Low-temperature PL spectra show interesting vibronic features that indicate exciton−phonon coupling and a single size or a narrow size distribution of the MCs. Furthermore, the MCs show good stability in the solid and solution states in the ambient environment. Structural studies based on Raman, XRD, and TEM led to the proposal of a layered structure of the MCs with a corner-shared tilted octahedral framework and the BTYA ligand coordinating to Pb^{2+} on the surface. This study demonstrates that the facile process made amino metal halide MCs retain their properties as isolated structures in solid form, making them promising for applications in devices in the future.

■ ASSOCIATED CONTENT

Supporting Information

The Supporting Information is available free of charge at https://pubs.acs.org/doi/10.1021/acs.jpclett.2c02977.

Details of materials and synthesis, spectroscopic measurements (UV−vis absorption, photoluminescence, and Raman spectra), XRD measurement, TEM measurement, control experiments for proof of formation of $PbBr_2$-BTYA MCs, and test of the stability of $PbBr_2$-BTYA MCs in the solid state (PDF)

■ AUTHOR INFORMATION

Corresponding Author

Jin Zhong Zhang − *Department of Chemistry and Biochemistry, University of California, Santa Cruz, California 95064, United States;* orcid.org/0000-0003-3437-912X; Email: zhang@ucsc.edu

Authors

Heng Zhang − *Department of Chemistry and Biochemistry, University of California, Santa Cruz, California 95064, United States*

Evan Thomas Vickers − *Department of Chemistry and Biochemistry, University of California, Santa Cruz, California 95064, United States; Nanoflow X, Carrollton, Texas 75006, United States*

Samuel Erickson − *Department of Physics, University of California, Merced, Merced, California 95343, United States*

Melissa Guarino-Hotz − *Department of Chemistry and Biochemistry, University of California, Santa Cruz, California 95064, United States;* orcid.org/0000-0001-6310-8156

Jeremy Lake Barnett − *Department of Chemistry and Biochemistry, University of California, Santa Cruz, California 95064, United States*

Sayantani Ghosh − *Department of Physics, University of California, Merced, Merced, California 95343, United States;* orcid.org/0000-0003-3440-7194

Complete contact information is available at: https://pubs.acs.org/10.1021/acs.jpclett.2c02977

Notes

The authors declare no competing financial interest.

■ ACKNOWLEDGMENTS

J.Z.Z. acknowledges financial support by the National Science Foundation (NSF, CHE-2203633). S.G. is grateful to funding from NSF (DGE-2125510) and NASA (MIRO NNX15AQ01A). X-ray diffraction was conducted at the X-ray Facility of the University of California, Santa Cruz, on the Rigaku Smartlab diffractometer (funded by NSF Grant MRI-1126845). TEM measurement was performed at the Molecular Foundry and supported by the Office of Science, Office of Basic Energy Sciences, of the U.S. Department of Energy under Contract DE-AC02-05CH11231. The authors thank David Strubbe for helpful discussions.

■ REFERENCES

(1) Zhou, C.; Lin, H.; Worku, M.; Neu, J.; Zhou, Y.; Tian, Y.; Lee, S.; Djurovich, P.; Siegrist, T.; Ma, B. Blue Emitting Single Crystalline Assembly of Metal Halide Clusters. *J. Am. Chem. Soc.* **2018**, *140* (41), 13181−13184.

(2) Vickers, E. T.; Chen, Z.; Cherrette, V.; Smart, T.; Zhang, P.; Ping, Y.; Zhang, J. Z. Interplay between Perovskite Magic-Sized Clusters and Amino Lead Halide Molecular Clusters. *Research* **2021**, *2021*, 1−7.

(3) Liu, L.; Pan, K.; Xu, K.; Peng, X.; Zhang, J. Z. Synthesis and Optical Properties of Mn^{2+}-Doped Amino Lead Halide Molecular Clusters Assisted by Chloride Ion. *J. Phys. Chem. Lett.* **2021**, *12* (31), 7497−7503.

(4) Protesescu, L.; Yakunin, S.; Bodnarchuk, M. I.; Krieg, F.; Caputo, R.; Hendon, C. H.; Yang, R. X.; Walsh, A.; Kovalenko, M. V. Nanocrystals of Cesium Lead Halide Perovskites ($CsPbX_3$, X = Cl, Br, and I): Novel Optoelectronic Materials Showing Bright Emission with Wide Color Gamut. *Nano Lett.* **2015**, *15* (6), 3692−3696.

(5) Pathak, S.; Sakai, N.; Wisnivesky Rocca Rivarola, F.; Stranks, S. D.; Liu, J.; Eperon, G. E.; Ducati, C.; Wojciechowski, K.; Griffiths, J. T.; Haghighirad, A. A.; et al. Perovskite Crystals for Tunable White Light Emission. *Chem. Mater.* **2015**, *27* (23), 8066−8075.
(6) Song, J.; Li, J.; Li, X.; Xu, L.; Dong, Y.; Zeng, H. Quantum Dot Light-Emitting Diodes Based on Inorganic Perovskite Cesium Lead Halides ($CsPbX_3$). *Adv. Mater.* **2015**, *27* (44), 7162−7167.
(7) Zhang, F.; Zhong, H.; Chen, C.; Wu, X.; Hu, X.; Huang, H.; Han, J.; Zou, B.; Dong, Y. Brightly Luminescent and Color-Tunable Colloidal $CH_3NH_3PbX_3$ (X = Br, I, Cl) Quantum Dots: Potential Alternatives for Display Technology. *ACS Nano* **2015**, *9* (4), 4533−4542.
(8) Hao, F.; Stoumpos, C. C.; Cao, D. H.; Chang, R. P. H.; Kanatzidis, M. G. Lead-Free Solid-State Organic−Inorganic Halide Perovskite Solar Cells. *Nat. Photonics* **2014**, *8* (6), 489−494.
(9) Liu, L.; Xu, K.; Vickers, E. T.; Allen, A.; Li, X.; Peng, L.; Zhang, J. Z. Varying the Concentration of Organic Acid and Amine Ligands Allows Tuning between Quantum Dots and Magic-Sized Clusters of $CH_3NH_3PbBr_3$ Perovskite: Implications for Photonics and Energy Conversion. *Acs Appl. Nano Mater.* **2020**, *3* (12), 12379−12387.
(10) Ning, J.; Banin, U. Magic Size InP and InAs Clusters: Synthesis, Characterization and Shell Growth. *Chem. Commun.* **2017**, *53* (17), 2626−2629.
(11) Mule, A. S.; Mazzotti, S.; Rossinelli, A. A.; Aellen, M.; Prins, P. T.; van der Bok, J. C.; Solari, S. F.; Glauser, Y. M.; Kumar, P. V.; Riedinger, A.; et al. Unraveling the Growth Mechanism of Magic-Sized Semiconductor Nanocrystals. *J. Am. Chem. Soc.* **2021**, *143* (4), 2037−2048.
(12) Aharonovich, I.; Englund, D.; Toth, M. Solid-State Single-Photon Emitters. *Nat. Photonics* **2016**, *10* (10), 631−641.
(13) Xu, K.; Vickers, E. T.; Luo, B.; Wang, Q.; Allen, A. C.; Wang, H.; Cherrette, V.; Li, X.; Zhang, J. Z. Room Temperature Synthesis of Cesium Lead Bromide Perovskite Magic Sized Clusters with Controlled Ratio of Carboxylic Acid and Benzylamine Capping Ligands. *Sol. Energy Mater. Sol. C* **2020**, *208*, 110341.
(14) Xu, K.; Allen, A. C.; Luo, B.; Vickers, E. T.; Wang, Q.; Hollingsworth, W. R.; Ayzner, A. L.; Li, X.; Zhang, J. Z. Tuning from Quantum Dots to Magic Sized Clusters of $CsPbBr_3$ Using Novel Planar Ligands Based on the Trivalent Nitrate Coordination Complex. *J. Phys. Chem. Lett.* **2019**, *10* (15), 4409−4416.
(15) Guarino-Hotz, M.; Barnett, J. L.; Pham, L. B.; Win, A. A.; Cherrette, V. L.; Zhang, J. Z. Tuning between Methylammonium Lead Bromide Perovskite Magic-Sized Clusters and Quantum Dots through Ligand Assisted Reprecipitation at Elevated Temperatures. *J. Phys. Chem. C* **2022**, *126* (32), 13854−13862.
(16) Li, H.; Yang, J.; Liang, C.; Zhang, W.; Zhou, M. Facile Electrochemical Synthesis of ZnO/PbSe Heterostructure Nanorod Arrays and PbSe Nanotube Arrays. *Appl. Surf. Sci.* **2012**, *258* (22), 8959−8964.
(17) Vickers, E. T.; Xu, K.; Dreskin, B. W.; Graham, T. A.; Li, X.; Zhang, J. Z. Ligand Dependent Growth and Optical Properties of Hybrid Organo-Metal Halide Perovskite Magic Sized Clusters. *J. Phys. Chem. C* **2019**, *123* (30), 18746−18752.
(18) Stamplecoskie, K. G.; Manser, J. S.; Kamat, P. V. Dual Nature of the Excited State in Organic−Inorganic Lead Halide Perovskites. *Energy Environ. Sci.* **2015**, *8* (1), 208−215.
(19) Naghadeh, S. B.; Sarang, S.; Brewer, A.; Allen, A.; Chiu, Y.-H.; Hsu, Y.-J.; Wu, J.-Y.; Ghosh, S.; Zhang, J. Z. Size and Temperature Dependence of Photoluminescence of Hybrid Perovskite Nanocrystals. *J. Chem. Phys.* **2019**, *151* (15), 154705.
(20) Smith, M. D.; Jaffe, A.; Dohner, E. R.; Lindenberg, A. M.; Karunadasa, H. I. Structural Origins of Broadband Emission from Layered Pb−Br Hybrid Perovskites. *Chem. Sci.* **2017**, *8* (6), 4497−4504.
(21) Dohner, E. R.; Jaffe, A.; Bradshaw, L. R.; Karunadasa, H. I. Intrinsic White-Light Emission from Layered Hybrid Perovskites. *J. Am. Chem. Soc.* **2014**, *136* (38), 13154−13157.
(22) Huang, S.; Yang, S.; Wang, Q.; Wu, R.; Han, Q.; Wu, W. $Cs_4PbBr_6/CsPbBr_3$ Perovskite Composites for WLEDs: Pure White, High Luminous Efficiency and Tunable Color Temperature. *RSC Adv.* **2019**, *9* (72), 42430−42437.
(23) Bryant, D.; Aristidou, N.; Pont, S.; Sanchez-Molina, I.; Chotchuangchutchaval, T.; Wheeler, S.; Durrant, J. R.; Haque, S. A. Correction: Light and Oxygen Induced Degradation Limits the Operational Stability of Methylammonium Lead Triiodide Perovskite Solar Cells. *Energy Environ. Sci.* **2016**, *9* (5), 1850−1850.
(24) Anaya, M.; Galisteo-López, J. F.; Calvo, M. E.; Espinós, J. P.; Míguez, H. Origin of Light-Induced Photophysical Effects in Organic Metal Halide Perovskites in the Presence of Oxygen. *J. Phys. Chem. Lett.* **2018**, *9* (14), 3891−3896.
(25) Wozny, S.; Yang, M.; Nardes, A. M.; Mercado, C. C.; Ferrere, S.; Reese, M. O.; Zhou, W.; Zhu, K. Controlled Humidity Study on the Formation of Higher Efficiency Formamidinium Lead Triiodide-Based Solar Cells. *Chem. Mater.* **2015**, *27* (13), 4814−4820.
(26) Zhu, Z.; Wu, Y.; Shen, Y.; Tan, J.; Shen, D.; Lo, M.-F.; Li, M.; Yuan, Y.; Tang, J.-X.; Zhang, W.; et al. Highly Efficient Sky-Blue Perovskite Light-Emitting Diode via Suppressing Nonradiative Energy Loss. *Chem. Mater.* **2021**, *33* (11), 4154−4162.
(27) Leguy, A. M. A.; Goñi, A. R.; Frost, J. M.; Skelton, J.; Brivio, F.; Rodríguez-Martínez, X.; Weber, O. J.; Pallipurath, A.; Alonso, M. I.; Campoy-Quiles, M.; et al. Dynamic Disorder, Phonon Lifetimes, and the Assignment of Modes to the Vibrational Spectra of Methylammonium Lead Halide Perovskites. *Phys. Chem. Chem. Phys.* **2016**, *18* (39), 27051−27066.
(28) Hu, Z.; Wang, X.; Wang, W.; Zhang, Z.; Gao, H.; Mao, Y. Raman Spectroscopy for Detecting Supported Planar Lipid Bilayers Composed of Ganglioside-GM1/Sphingomyelin/Cholesterol in the Presence of Amyloid-β. *Phys. Chem. Chem. Phys.* **2015**, *17* (35), 22711−22720.
(29) Jia, Q.-Q.; Tong, L.; Lun, M.-M.; Fu, D.-W.; Zhang, T.; Lu, H.-F. Two-Dimensional Organic−Inorganic Hybrid Materials with Dielectric Switching and Photoluminescence Properties. *Cryst. Growth Des.* **2022**, *22* (5), 2799−2805.
(30) Xu, L.-J.; Worku, M.; He, Q.; Lin, H.; Zhou, C.; Chen, B.; Lin, X.; Xin, Y.; Ma, B. Ligand-Mediated Release of Halides for Color Tuning of Perovskite Nanocrystals with Enhanced Stability. *J. Phys. Chem. Lett.* **2019**, *10* (19), 5836−5840.
(31) Wang, H.; Zhao, X.; Zhang, B.; Xie, Z. Blue Perovskite Light-Emitting Diodes Based on RbX-Doped Polycrystalline $CsPbBr_3$ Perovskite Films. *J. Mater. Chem. C* **2019**, *7* (19), 5596−5603.
(32) Weidman, M. C.; Seitz, M.; Stranks, S. D.; Tisdale, W. A. Highly Tunable Colloidal Perovskite Nanoplatelets through Variable Cation, Metal, and Halide Composition. *ACS Nano* **2016**, *10* (8), 7830−7839.
(33) Chang, Y.-H.; Lin, J.-C.; Chen, Y.-C.; Kuo, T.-R.; Wang, D.-Y. Facile Synthesis of Two-Dimensional Ruddlesden−Popper Perovskite Quantum Dots with Fine-Tunable Optical Properties. *Nanoscale Res. Lett.* **2018**, *13* (1), 247.
(34) Dou, L. Emerging Two-Dimensional Halide Perovskite Nanomaterials. *J. Mater. Chem. C* **2017**, *5* (43), 11165−11173.
(35) Era, M.; Kobayashi, T.; Noto, M. PbBr-Based Layered Perovskite Organic−Inorganic Superlattice Having Hole-Transporting Carbazole Chromophore in Organic Layer. *Curr. Appl. Phys.* **2005**, *5* (1), 67−70.
(36) Sengupta, A.; Mandal, K. C.; Zhang, J. Z. Ultrafast Electronic Relaxation Dynamics in Layered Iodide Semiconductors: A Comparative Study of Colloidal BiI_3 and PbI_2 Nanoparticles. *J. Phys. Chem. B* **2000**, *104* (40), 9396−9403.
(37) Tian, Y.; Zhou, C.; Worku, M.; Wang, X.; Ling, Y.; Gao, H.; Zhou, Y.; Miao, Y.; Guan, J.; Ma, B. Light-Emitting Diodes: Highly Efficient Spectrally Stable Red Perovskite Light-Emitting Diodes. *Adv. Mater.* **2018**, *30* (20), 1870142.

https://doi.org/10.1021/acs.jpclett.2c02977
J. Phys. Chem. Lett. 2022, 13, 10543−10549